Original Research

Prostate Cancer Screening: The Clinical Value of Diffusion-Weighted Imaging and Dynamic MR Imaging in Combination with T2-Weighted Imaging

Akihiro Tanimoto, MD,[1]* Jun Nakashima, MD,[2] Hidaka Kohno, MD,[2] Hiroshi Shinmoto, MD,[1] and Sachio Kuribayashi, MD[1]

Purpose: To evaluate the clinical value of diffusion-weighted imaging (DWI) and dynamic MRI in combination with T2-weighted imaging (T2W) for the detection of prostate cancer.

Materials and Methods: A total of 83 patients with elevated serum prostate specific antigen (PSA) levels (>4.0 ng/mL) were evaluated by T2W, DWI, and dynamic MRI at 1.5 T prior to needle biopsy. The data from the results of the T2W alone (protocol A), combination of T2W and DWI (protocol B), and the combination of T2W+DWI and dynamic MRI (protocol C) were entered into a receiver operating characteristic (ROC) curve analysis, under results of systemic biopsy as the standard of reference.

Results: Prostate cancer was pathologically detected in 44 of the 83 patients. The sensitivity, specificity, accuracy, and the area under the ROC curve (Az) for the detection of prostate cancer were as follows: 73%, 54%, 64%, and 0.711, respectively, in protocol A; 84%, 85%, 84%, and 0.905, respectively, in protocol B; and 95%, 74%, 86%, and 0.966, respectively, in protocol C. The sensitivity, specificity, and accuracy were significantly different between the three protocols ($P < 0.01$).

Conclusion: In patients with elevated serum PSA levels, the combination of T2W, DWI, and dynamic MRI may be a valuable tool for detecting prostate cancer and avoiding an unnecessary biopsy without missing prostate cancer.

Key Words: prostate; neoplasm; MRI; diffusion; dynamic study
J. Magn. Reson. Imaging 2007;25:146–152.

PROSTATE CANCER is the most frequent malignant tumor in the male population of the United States, and its incidence is rapidly increasing in Japan (1). Recently, prostate-specific antigen (PSA), which has been identified as a useful tumor marker, and transrectal ultrasound (TRUS) have facilitated the detection of early-stage prostate cancer, by screening candidates for systematic biopsy. However, the positive predictive value (PPV) of the elevated PSA levels or TRUS-guided biopsy is relatively low. It has been documented that only 25% of patients with gray-zone PSA levels may have prostate cancer (2). Other authors have reported that the PPV for PSA and digital rectal examination were 32% and 21%, respectively (3). TRUS-guided biopsy cores showed 42% positive and 58% negative (4). Recent studies have suggested the usefulness of newer ultrasound (US) techniques such as color Doppler US, power Doppler US, and contrast-enhanced US; however, these techniques are still under development (5–7).

Avoiding unnecessary biopsies without missing prostate cancer in men with elevated serum PSA levels is an aspect that requires focus. An unnecessary biopsy can be avoided by the accurate detection and localization of prostate cancer. This will also facilitate targeted biopsy, which has a higher detection rate than conventional sextant biopsies (8). In this study, we evaluated the clinical value of diffusion-weighted imaging (DWI) and dynamic MRI in combination with T2-weighted imaging (T2W) for the screening of prostate cancer in patients with elevated PSA levels.

MATERIALS AND METHODS

Patients

Between January and May 2005, 83 consecutive male patients with elevated PSA levels (>4.0 ng/mL) who had undergone both an MRI and a subsequent systematic transrectal prostate biopsy were included in this study. The patients' ages ranged from 53 to 87 years (mean age 67.4 years). This study followed the Declaration of Helsinki principles, and urologists explained the purpose of the diagnostic MRI to each patient and obtained their written informed consent. In our study population, 19 of 83 patients (3 of 39 noncancerous patients and 16 of 44 cancerous patients) showed positive digital rectal

[1]Department of Diagnostic Radiology, School of Medicine, Keio University, Tokyo, Japan.
[2]Department of Urology, School of Medicine, Keio University, Tokyo, Japan.
*Address reprint requests to: A.T., M.D., Department of Diagnostic Radiology, School of Medicine, Keio University, 35 Shinanomachi, Shinjuku-ku, Tokyo 160-8582, Japan. E-mail: t-mri@tt.rim.or.jp
Received November 23, 2005; Accepted August 31, 2006.
DOI 10.1002/jmri.20793
Published online 30 November 2006 in Wiley InterScience (www.interscience.wiley.com).

exam (DRE). Biopsies were performed on all the patients within four months after MRI examination. In 44 of the 83 patients, systematic biopsies for the prostate revealed the existence of cancerous tissues. In this study, the standard of reference was determined by the results of systematic biopsy. If any biopsy specimen from a patient showed pathologically positive results, the patient was considered "true positive." Conversely, patients showing negative biopsy results were considered "true negative." During the study period, 10 of the 44 patients with cancer underwent radical prostatectomy.

MRI

Patients underwent MRI on a 1.5-Tesla MR scanner (Signa Excite XI; GE Healthcare, Hino, Japan). Oblique-axial imaging planes were determined to be the short axis of the prostate in the sagittal localizing scan, such that approximately 10 sections were obtained for each patient. T2W fast spin echo (FSE): TR/TE = 5000 msec/87.9 msec, echo train length = 18, matrix sizes = 288 × 192, number of excitations (NEX) = 4, acquisition time = 3 minutes 45 seconds), T1-weighted FSE (TR/TE = 560 msec/12 msec, echo train length = 2, matrix sizes = 256 × 192, NEX = 2, acquisition time = 1 minute 50 seconds), diffusion-weighted single-shot echo planar imaging (SSEPI) (TR/TE = 3600 msec/72.6 msec, matrix sizes = 160 × 128, NEX = 8, acquisition time = 1 minute 55 seconds), and gadolinium-enhanced dynamic MRI (fat-suppressed fast spoiled gradient-recalled acquisition in steady state (FSPGR): TR/TE/flip angle = 130 msec/2.0 msec/90°, matrix sizes = 256 × 160, NEX = 1, acquisition time = 22 seconds) were performed using eight-channel torso-array coils. In diffusion-weighted SSEPI, images were obtained by using diffusion gradients with two b-values (0 and 1000 seconds/mm^2) along the three directions of the motion-probing gradients (9). A parallel imaging technique, array spatial sensitivity encoding technique (ASSET), was used with a reduction factor of two. In dynamic scans, precontrast baselines, 40 and 180 seconds after bolus injection of 0.1 mmol/kg of gadopentetate dimeglumine (Magnevist; Nihon Schering, Osaka, Japan) were sequentially obtained. The timing of image acquisition in the dynamic study was referred to the time-enhancement curves of benign and malignant prostate tissue at dynamic MRI by Rouviere et al (10). The field of view was 36 cm in diffusion-weighted echo planar imaging (EPI), and 18 cm for other sequences. The slice thickness/interslice gap was 5 mm/0.5 mm for all sequences.

Image Interpretation

Receiver Operating Characteristic (ROC) Curve Analysis

We analyzed three image interpretation protocols. Protocol A consisted of data from T2W-FSE alone, protocol B consisted of T2W-FSE plus DWI, and protocol C consisted of T2W-FSE plus DWI along with dynamic MRI. All image interpretation sessions were performed on a workstation (AW version 4.1; GE Healthcare). For DWI, the apparent diffusion coefficient (ADC) maps and/or exponential ADC (eADC) maps were constructed on the workstation and simultaneously displayed to the readers during the image interpretation session. The eADC was defined as exp (–b × ADC), and the color shades used on the ADC map were inverted. The ability of each imaging protocol for the detection of prostate cancer was evaluated by means of ROC analyses (11). Each dataset was reviewed with the consensus of two readers after a minimum interval of two weeks to avoid decision threshold bias due to reading-order effects. For each dataset (oblique axial sections covering the entire prostate) from each patient, a confidence score reflecting the perceived likelihood of the presence of cancer was assigned using the following five-point scale: 5, definitely positive; 4, probably positive; 3, possibly positive; 2, probably negative; and 1, definitely negative. By plotting the true-positive fraction (TPF) on the ordinate and the probability of a false positive on the abscissa, the area under the ROC curve (Az) was calculated by using the maximum-likelihood estimation (ROCKIT version 0.9B1 for Macintosh to calculate Az in ROC analysis; courtesy of Charles E. Metz at the University of Chicago, Chicago, IL, USA (12)). The 44 patients who were histopathologically confirmed to have cancer served as true positives, and the other 39 patients without evidence of prostate cancer served as true negatives. To calculate the sensitivity, specificity, and accuracy of each modality, scores of 5, 4, and 3 were considered positive findings, and scores of 1 and 2 were considered negative findings.

Diagnostic Criteria

When T2W-FSE was used, a low signal intensity in the peripheral zone (PZ), accompanied by the disruption of the duct structure, was considered malignant (rank 5), while a symmetrical, wedge-shaped low signal intensity with maintained duct structure was considered noncancerous (rank 1 or 2). In case of the transition zone (TZ), an irregular low signal intensity area without a capsule, or a signal intensity obliterating normal structures such as the surgical capsule or the urethra, were considered malignant.

When DWI was used, any lesions in the PZ showing a decrease in the ADC was considered malignant. If the lesion showed an apparently cold color (blue) on the ADC map or a warm color (red) on the eADC map, it was assigned a rank of 5. If the color was moderately cold or warm, it was assigned a rank of 3 or 4. If the lesions were less than 5 mm in size and were located in the TZ, they were not considered and were assigned a rank of 1 or 2.

When dynamic MRI was used, lesions showing enhancements in the early phase and a washout in the delayed phase were considered positive (rank 5). Lesions showing early and prolonged enhancement were suspected of being malignancy (rank 3 or 4). Lesions that did not show early enhancement but showed a gradual enhancement in the delayed phase were not considered (rank 1 or 2).

ADC Value Measurements

For nine of the 10 patients who underwent radical prostatectomy, histopathological hematoxylin and eosin (H&E) stains from the entire prostate tissue were prepared to measure the ADC. One patient who had undergone neoadjuvant endocrine therapy prior to prostatectomy was excluded from the measurements and no cancer cells were detected in the histopathological specimen. To measure the ADC of each tissue, accurate placement of the region of interest (ROI) circle on the ADC maps was ensured at the regions corresponding to the cancerous tissues and noncancerous PZ and TZ tissues in the histopathological sections. For cancerous tissue, the ROI circle was placed in the cancerous area as large as possible (minimum ROI circle diameter was 5 mm in our series, such that the minimum area of ROI circle was 19.6 mm^2), with referring to the histopathological sections. To avoid any other tissues in ROI, we referred to T2W MR images and/or dynamic MR images of this study. For the accurate ADC measurement, every effort was made to put the ROI circle on each tissue as large as possible through the measurements. The type of hyperplasia in TZ was not considered in placing the ROI circle.

On the workstation, the ADC value of each pixel was constantly displayed on the screen with movement of the cursor, and the minimum ADC value from a pixel of each tissue was recorded for this subset of nine patients. The color shades on the ADC maps also identified the pixel showing the minimum ADC value. Regions of low ADC showed a cold color (blue); in contrast, regions of high ADC showed a warm color (red).

Statistical Analysis

Statistical analysis was performed on a Power Macintosh G4 computer (Apple Computer Japan Co., Tokyo, Japan) by using Statview (version 4.5, Hulinks Co., Tokyo, Japan) and Statcel (OMS Ltd., Saitama, Japan). The Az values of the three protocols were compared by using the ROCKIT program (two-variable chi-squared test), and the 95% confidence intervals (CI) were calculated (12). The sensitivity, specificity, and accuracy of the three imaging protocols were compared by using the Cochran-Q test, and that between any two protocols by using the McNemar test (13). A P value of 0.05 or less was considered to indicate a statistically significant difference between the three protocols, and a P value of 0.016 after the Bonferroni correction was considered statistically significant in the comparison between any two protocols (14). For the comparison of the ADC values between cancerous tissues, noncancerous PZ tissues, and noncancerous TZ tissues, a randomized blocks method was used. This method evaluated the difference between the three tissues, and a post-hoc test (Tukey's test) was used to compare the ADC values of any two tissues.

RESULTS

PSA Levels and Histopathological Finding

PSA levels in 83 patients ranged from 4.3 to 332.1 ng/mL (19.4 ± 43.5 ng/mL [mean ± SD]). In 44 patients with cancer, 23 had a PSA level of 4–10 ng/mL, 12 had a level of 10–20 ng/mL, and nine had a level of >20 ng/mL, such that the mean PSA was 28.6 ± 58.1 ng/mL. In 39 noncancerous patients, 31 had a PSA level of 4–10 ng/mL, five had a level of 10–20 ng/mL, and three had a level of >20 ng/mL, such that the mean PSA was 9.0 ± 6.8 ng/mL. A total of 23 of the 54 patients with gray zone PSA levels (4–10 ng/mL) and 21 of the 29 patients with PSA levels above 10 ng/mL were confirmed to have cancer. Between patients with gray zone PSA and patients with higher PSA levels (>10 ng/mL), there was a significant difference in pathological results (cancerous or noncancerous), by Fisher's exact probability test (P = 0.008).

The Gleason's scores of cancerous tissue in the study population were as follows: 15 of 44 patients with cancer showed a Gleason's score of 6 and below (score of 4 in two patients, score of 5 in eight, score of 6 in five, score of 7 in 15, score of 8 in four, and score of 9 in 10). The mean score of cancerous tissue was 6.9. In a subset of 10 patients who had undergone radical prostatectomy, seven had moderately differentiated adenocarcinoma, two had well differentiated adenocarcinoma, and one who received neoadjuvant endocrine therapy had no cancer cells in the specimen.

ADC Measurements

In a subset of radical prostatectomy, the mean ADC ($\times 10^{-3}$ mm^2/second) was 0.93 ± 0.11 (range = 0.89–1.14) for the cancerous tissue, 1.72 ± 0.35 (range = 1.25–2.29) for the noncancerous PZ tissue, and 1.46 ± 0.16 (range = 1.18–1.63) for the noncancerous TZ tissue (Fig. 2). A randomized blocks method indicated a significant difference between the three tissues (P = 0.000003). Post-hoc test (Tukey's test) revealed that cancerous tissues showed significantly lower ADC values than those of noncancerous PZ or TZ tissues ($P <$ 0.001). The minimum ADC value of the cancerous tissue was 0.72 ± 0.19 (range = 0.39–0.93). No difference was noted in ADC values of cancerous tissue in nine cases of radical prostatectomy. In six cases with a Gleason's score of 7, ADC values ranged from 0.795 to 1.140. In two cases with a score of 6, ADC values were 0.833 and 1.020. In one case with a score of 5, the ADC was 0.963.

MR Diagnostic Performance

In the ROC analyses, the Az values were 0.711 (95% CI = 0.590–0.813), 0.905 (95% CI = 0.815–0.957), and 0.966 (95% CI = 0.914–0.989) for protocols A, B, and C, respectively (Fig. 1). There were significant differences between protocols A and B (P = 0.011) and between protocols A and C (P = 0.0003). Although a tendency to differ was observed between protocols B and C, the difference was not statistically significant (P = 0.084).

The sensitivity, specificity, and accuracy for the detection of prostate cancer were 73%, 54%, and 64%, respectively, in protocol A; 84%, 85%, and 84%, respectively, in protocol B; and 95%, 74%, and 86%, respectively, in protocol C. The sensitivity, specificity, and

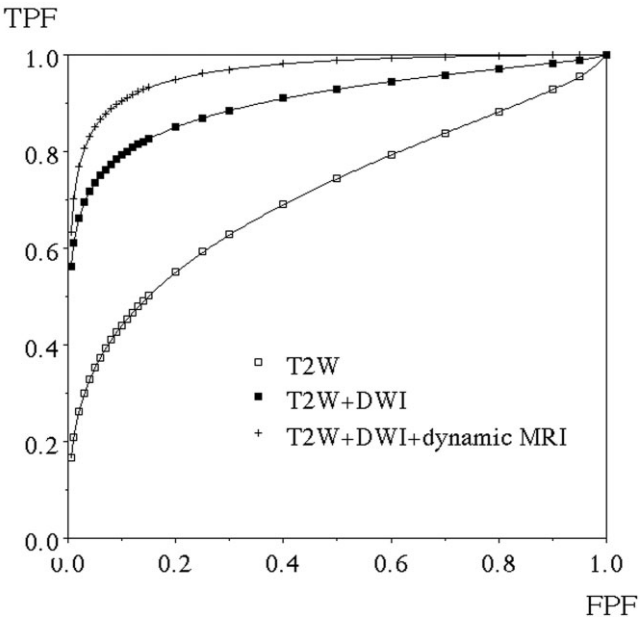

Figure 1. The ROC curve of the three protocols.

accuracy were significantly different between the three protocols (Cochran-Q test: $P = 0.009$, $P = 0.009$, and $P = 0.0005$, respectively). The sensitivity and accuracy were significantly different between protocols A and C (McNemar test: $P = 0.014$ and $P = 0.003$, respectively), and the specificity and accuracy were significantly different between protocols A and B (McNemar test: $P = 0.014$ and $P = 0.003$, respectively). Some representative cases are shown in Figs. 3–5.

DISCUSSION

T2W shows excellent tissue contrast in the prostate, and the zonal anatomy advocated by McNeal (15) can be clearly identified (16). The inherent zonal T2 contrast of the prostate makes cancer detection in the PZ relatively easy, but the detection is often difficult in the inner gland. MRI with endorectal surface coil has been used for the delineation of the extent of extracapsular cancer and seminal vesicle invasion, or for posttherapeutic checkup, but the technique has not been applied for the screening of cancer (17–19). In addition, postbiopsy hemorrhage shows low signal intensity on T2W and frequently masks cancerous tissues (20). Proton MR spectroscopy (MRS) can be considered a tool to detect prostate cancer (21,22), but this technique requires new MR equipment and prolonged examination time; moreover, multicenter trials have not fully established its clinical value.

DWI has been applied for early detection of brain ischemia over the last decade (23). The ADC measurement has also been known to be useful for distinguishing between benign and malignant lesions (24); however, the application of DWI to body MRI was limited due to motion/susceptibility artifacts. However, the recent developments to improve MRI enabled the use of DWI for the body due to high b-values in DWI and parallel imaging techniques (25–27). Some preliminary studies have indicated that DWI can distinguish prostate cancer tissues from benign tissues because of the differences in the ADC values (28–30). Our results indicated a significant difference in the ADC values between cancerous and noncancerous tissues, similar to Sato et al (30). Although the b-values (0 and 1000 second/mm^2) in our study were different from those reported by Sato et al (30) (0, 300, and 600 second/mm^2), the range of obtained ADC values was similar. However, the b-values should be optimized for accurately detecting prostate cancer and establishing the reproducibility of ADC measurement when different MR equipment is used. Our ADC data, based on the entire prostate specimen, would be more reliable than ADC data based on biopsy results. Although in a small number of cases the cutoff value of the mean ADC between cancerous and noncancerous tissues ranged from 1.14 to 1.18 ($\times 10^{-3}$ mm^2/second) and the minimum ADC pixel value of cancer was below 0.93 ($\times 10^{-3}$ mm^2/second), these data provided some objectivity in the interpretation of the ADC map. In addition, the use of ADC maps together with DWI would be recommended. In our study, areas with low ADC were more easily recognized on color ADC maps than on DWI alone, although prostate cancer usually shows low signal intensity on T2W and therefore T2 shine-through could almost be neglected in the interpretation of DWI.

Preliminary studies have shown that prostate cancer tissues enhanced earlier than the normal PZ tissues (24), but the usefulness of dynamic MRI in depicting prostate cancer remains controversial because of an overlap in enhancement patterns between normal and cancerous tissues (31–33). In particular, the optimum imaging period after gadolinium injection remains unknown; moreover, thus far, there is limited information on the time-enhancement curves of prostate cancer and the normal surrounding tissues (32–33). Recently, quantitative analyses using the time-intensity curve or the tracer kinetic model have been reported (10,34,35). Preziosi et al (34) reported that the time period between

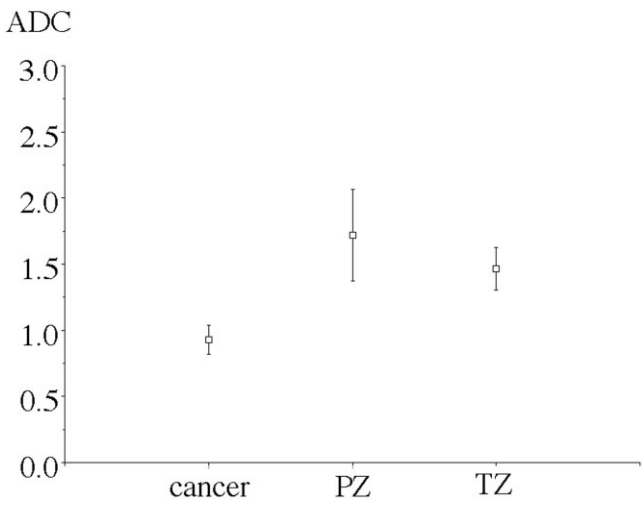

Figure 2. The ADC values of cancerous tissues, noncancerous PZ tissues, and noncancerous TZ tissues ($\times 10^{-3}$ mm^2/second).

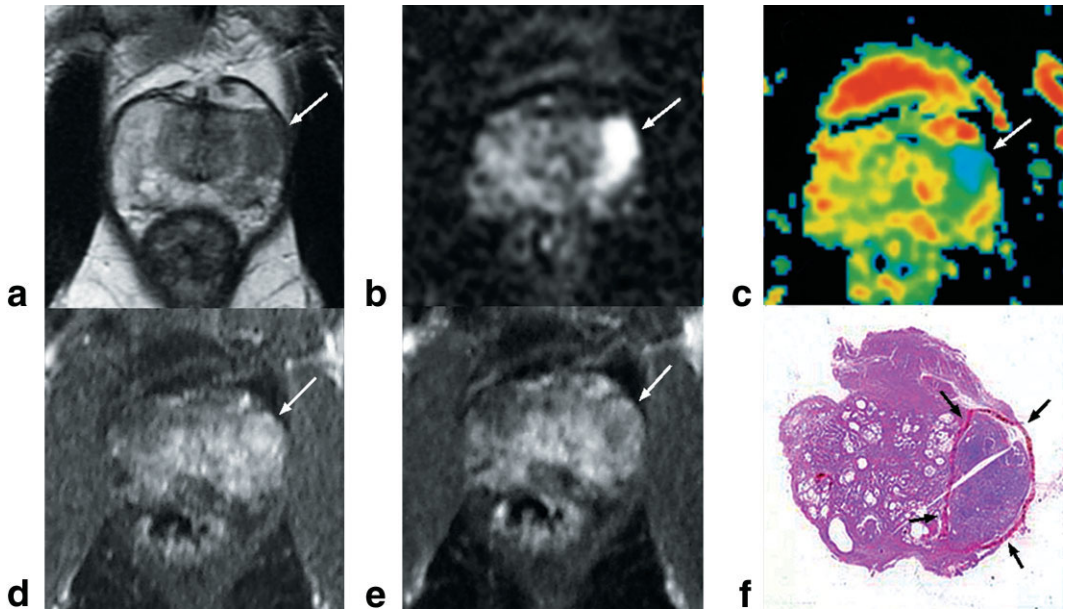

Figure 3. A 59-year-old male with prostate cancer (moderately differentiated adenocarcinoma, Gleason's score 3 + 4 = 7, capsule invasion (–)). When T2W was used, a low intensity area is noted in the left lobe of the prostate (**a**, arrow). DWI (**b**, arrow) and ADC map (**c**, arrow) clearly demonstrate decreased diffusion. The lesion is well enhanced in the early phase of dynamic study (**d**, arrow). In delayed phase, the lesion showed washout (**e**, arrow). The minimum ADC of the lesion is 0.60×10^{-3} mm^2/second. During image interpretation sessions, a rank of 5 was assigned for all three protocols. A histopathological H&E stain section showed the cancerous area corresponding to the MR image findings (**f**, arrows).

the bolus injection and the maximum intensity in cancerous tissue ranged 70–180 seconds (mean = 103 seconds), whereas that in noncancerous tissue ranged 200–300 seconds (mean = 250 seconds). In our protocol, the scan time of dynamic MRI was 22 seconds and the delay time was 40–180 seconds, which seemed to be a reasonable imaging window to enable peak enhancement of cancer.

Recently, Shimofusa et al (9) reported that prostate cancer could be detected more accurately by T2W with DWI as compared with T2W alone. Their study was conducted retrospectively, and they concluded that

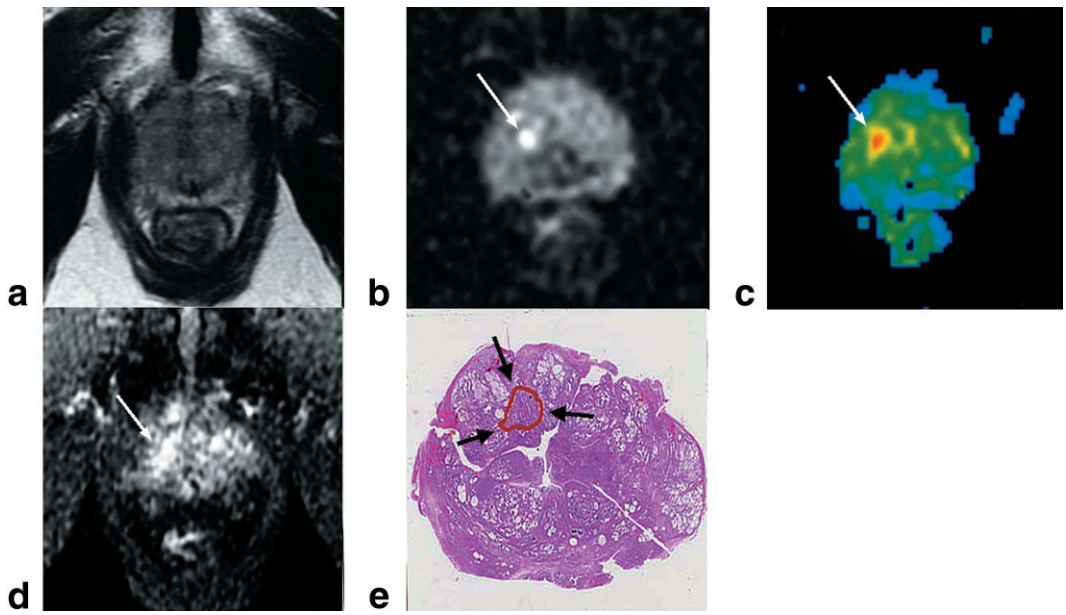

Figure 4. A 67-year-old male with prostate cancer (moderately differentiated adenocarcinoma, Gleason's score 3 + 4 = 7, capsule invasion (–)); a case of TZ cancer. No abnormal finding was observed when T2W was used, and a rank of 1 was assigned (**a**). However, DWI (**b**, arrow), eADC map (**c**, arrow), and dynamic MRI (**d**, arrow) clearly demonstrate the presence of a lesion in the right lobe. The minimum ADC of the lesion is 0.66×10^{-3} mm^2/second. In protocols B and C, a rank of 5 was assigned. A histopathological H&E stain section showed the cancerous area corresponding to the MR image findings (**e**, arrows).

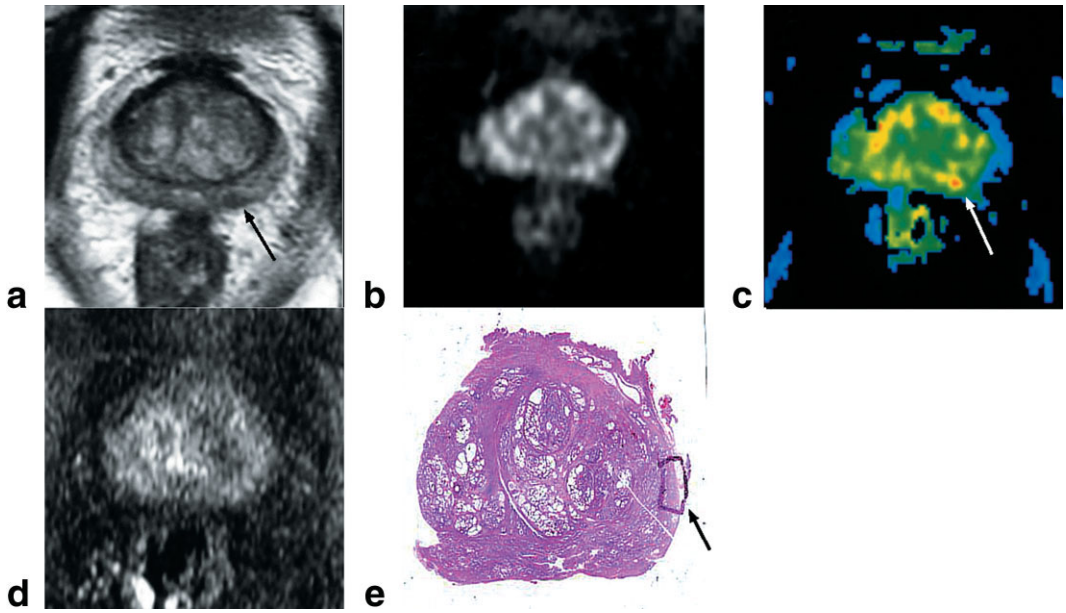

Figure 5. A 54-year-old male with prostate cancer (well-differentiated adenocarcinoma, Gleason's score 3 + 3 = 6, capsule invasion (±)). When T2W was used, presence of a small low intensity area is barely noted prospectively (**a**, arrow). The lesion is unclear on DWI (**b**) and dynamic MRI (**d**), but it is retrospectively noted on the eADC map (**c**, arrow). The minimum ADC of the lesion is 0.84×10^{-3} mm^2/second. During the image interpretation sessions, a rank of 3 was assigned for protocol A and a rank of 2 for protocols B and C. A histopathological H&E stain section showed the cancerous area corresponding to the MR image findings (**e**, arrow).

combining DWI with T2W provided better detection of prostate cancer. Our preliminary study used visual inspection alone for image interpretation and proposed a simple and practical screening method for prostate cancer. To our knowledge, this is the first prospective study to screen for prostate cancer among patients with elevated PSA levels. The influence of postbiopsy hemorrhage on the MRI findings can be excluded. The examination time including time spent on patient preparation was approximately 20 minutes, which was favorable for patient throughput. Application of this method to the local staging of cancer and follow-up for posttherapeutic patients will be the focus areas for subsequent studies.

There are some limitations in our study. First, some patients who were not considered to have cancer may actually have prostate cancer, because the presence of cancer was judged by systematic biopsy alone in a majority of the cases. Second, MRI findings do not correspond directly to the biopsy results since the entire prostate specimen was not compared. Third, well-differentiated adenocarcinoma confirmed in the radical prostatectomy showed ambiguous MRI findings (Fig. 5); however, correlations between the Gleason's scores and the MRI findings were not fully investigated. Last, there might be some image interpretation bias caused by the reading order of the pulse sequences, because addition of dynamic MRI slightly improved sensitivity, accuracy, and Az in the ROC curve but worsened the specificity to some extent. Further studies will be required to assess the merits and demerits of dynamic MRI, including quantitative image analysis.

In conclusion, in patients with elevated serum PSA levels, the combination of DWI and dynamic MRI with T2W may facilitate the detection of prostate cancer as compared with T2W alone. Therefore, the combination of T2W, DWI, and dynamic MRI may be a valuable tool for the detection of prostate cancer while avoiding an unnecessary biopsy without missing prostate cancer.

REFERENCES

1. Quinn M, Babb P. Patterns and trends in prostate cancer incidence, survival, prevalence and mortality. Part II: Individual countries. BJU Int 2002;90:174–184.
2. Brawer MK. Prostate-specific antigen: Current status. CA Cancer J Clin 1999;49:264–281.
3. Loch T, Eppelmann U, Lehmann J, Wullich B, Loch A, Stockle M. Transrectal ultrasound guided biopsy of the prostate: random sextant versus biopsies of sono-morphologically suspicious lesions. World J Urol 2004;22:357–360.
4. Catalona WJ, Richie JP, Ahmann FR, et al. Comparison of digital rectal examination and serum prostate specific antigen in the early detection of prostate cancer: results of a multicenter clinical trial of 6,630 men. J Urol 1994;151:1283–1290.
5. Arger PH, Malkowicz SB, VanArsdalen KN, Sehgal CM, Holzer A, Schultz SM. Color and power Doppler sonography in the diagnosis of prostate cancer: comparison between vascular density and total vascularity. J Ultrasound Med 2004;23:623–630.
6. Halpern EJ, Rosenberg M, Gomella LG. Prostate cancer: contrast-enhanced US for detection. Radiology 2001:219:219–225.
7. Halpern EJ, Frauscher F, Forsberg F, et al. Prostate: high-frequency Doppler US imaging for cancer detection. Radiology 2002: 225:71–77.
8. Kravchick S, Cytron S, Peled R, London D, Sibi Y, Ben-Dor D. Optimal combinations for detection of prostate cancer: systematic sextant and laterally directed biopsies versus systematic sextant and color Doppler-targeted biopsies. Urology 2004;63:301–305.
9. Shimofusa R, Fujimoto H, Akamata H, et al. Diffusion-weighted imaging of prostate cancer. J Comput Assist Tomogr 2005;29:149–153.
10. Rouviere O, Raudrant A, Ecochard R, et al. Characterization of time-enhancement curves of benign and malignant prostate tissue at dynamic MR imaging. Eur Radiol 2003;13:931–942.

11. Metz CE. Basic principles of ROC analysis. Semin Nucl Med 1978; 8:283–298.
12. ROCKIT software. Kurt Rossmann Laboratories for Radiologic Image Research, University of Chicago, Chicago, IL, USA. Available at: http://www-radiology.uchicago.edu/krl/roc_soft5.htm. Last accessed: October 6, 2006.
13. Dwyer AJ. Matchmaking and McNemar in the comparison of diagnostic modalities. Radiology 1991;178:328–330.
14. Bonferroni correction. Wolfram MathWorld. Wolfram Research, Inc., Champaign, IL, USA. Available at: http://mathworld.wolfram.com/BonferroniCorrection.html. Last accessed: October 6, 2006.
15. McNeal JE. The zonal anatomy of the prostate. Prostate 1981;2:35–49.
16. Hricak H, Dooms GC, McNeal JE, et al. MR imaging of the prostate gland: normal anatomy. AJR Am J Roentgenol 1987;148:51–58.
17. Hricak H, White S, Vigneron D, et al. Carcinoma of the prostate gland: MR imaging with pelvic phased-array coils versus integrated endorectal-pelvic phased-array coils. Radiology 1994;193:703–709.
18. Presti JC Jr, Hricak H, Narayan PA, Shinohara K, White S, Carroll PR. Local staging of prostatic carcinoma: comparison of transrectal sonography and endorectal MR imaging. AJR Am J Roentgenol 1996;166:103–108.
19. Chen M, Hricak H, Kalbhen CL, et al. Hormonal ablation of prostatic cancer: effects on prostate morphology, tumor detection, and staging by endorectal coil MR imaging. AJR Am J Roentgenol 1996; 166:1157–1163.
20. White S, Hricak H, Forstner R, et al. Prostate cancer: effect of postbiopsy hemorrhage on interpretation of MR images. Radiology 1995;195:385–390.
21. Kurhanewicz J, Swanson MG, Nelson SJ, Vigneron DB. Combined magnetic resonance imaging and spectroscopic imaging approach to molecular imaging of prostate cancer. J Magn Reson Imaging 2002;16:451–463.
22. Prando A, Kurhanewicz J, Borges AP, Oliveira EM Jr, Figueiredo E. Prostatic biopsy directed with endorectal MR spectroscopic imaging findings in patients with elevated prostate specific antigen levels and prior negative biopsy findings: early experience. Radiology 2005;236:903–910.
23. Minematsu K, Li L, Fisher M, Sotak CH, Davis MA, Fiandaca MS. Diffusion-weighted magnetic resonance imaging: rapid and quantitative detection of focal brain ischemia. Neurology 1992;42:235–240.
24. Herneth AM, Guccione S, Bednarski M. Apparent diffusion coefficient: a quantitative parameter for in vivo tumor characterization. Eur J Radiol 2003;45:208–213.
25. Takahara T, Imai Y, Yamashita T, Yasuda S, Nasu S, Van Cauteren M. Diffusion weighted whole body imaging with background body signal suppression (DWIBS): technical improvement using free breathing, STIR and high resolution 3D display. Radiat Med 2004; 22:275–282.
26. Kuroki Y, Nasu K, Kuroki S, et al. Diffusion-weighted imaging of breast cancer with the sensitivity encoding technique: analysis of the apparent diffusion coefficient value. Magn Reson Med Sci 2004; 3:79–85.
27. Nakayama T, Yoshimitsu K, Irie H, et al. Diffusion-weighted echo-planar MR imaging and ADC mapping in the differential diagnosis of ovarian cystic masses: usefulness of detecting keratinoid substances in mature cystic teratomas. J Magn Reson Imaging 2005; 22:271–278.
28. Issa B. In vivo measurement of the apparent diffusion coefficient in normal and malignant prostatic tissues using echo-planar imaging. J Magn Reson Imaging 2002;16:196–200.
29. Hosseinzadeh K, Schwarz SD. Endorectal diffusion-weighted imaging in prostate cancer to differentiate malignant and benign peripheral zone tissue. J Magn Reson Imaging 2004;20:656–661.
30. Sato C, Naganawa S, Nakamura T, et al. Differentiation of noncancerous tissue and cancer lesions by apparent diffusion coefficient values in transition and peripheral zones of the prostate. J Magn Reson Imaging 2005;21:258–262.
31. Liney GP, Turnbull LW, Knowles AJ. In vivo magnetic resonance spectroscopy and dynamic contrast enhanced imaging of the prostate gland. NMR Biomed 1999;12:39–44.
32. Jager GJ, Ruijter ETG, Kaa CA, et al. Dynamic TurboFLASH subtraction technique for contrast-enhanced MR imaging of the prostate: correlation with histopathologic results. Radiology 1997;203: 645–652.
33. Turnbull LW, Buckley DL, Turnbull LS, Liney GP, Knowles AJ. Differentiation of prostatic carcinoma and benign prostatic hyperplasia: correlation between dynamic Gd-DTPA-enhanced MR imaging and histopathology. J Magn Reson Imaging 1999;9:311–316.
34. Preziosi P, Orlacchio A, Di Giambattista G, et al. Enhancement patterns of prostate cancer in dynamic MRI. Eur Radiol 2003;13: 925–930.
35. Buckley DL, Roberts C, Parker GJ, Logue JP, Hutchinson CE. Prostate cancer: evaluation of vascular characteristics with dynamic contrast-enhanced T1-weighted MR imaging-initial experience. Radiology 2004;233:709–715.